

Cite this: *Dalton Trans.*, 2019, **48**, 17371

A functionalized UiO-66 MOF for turn-on fluorescence sensing of superoxide in water and efficient catalysis for Knoevenagel condensation†

Aniruddha Das,^a Nagaraj Anbu,^{‡b} Mostakim SK,^{‡a} Amarajothi Dhakshinamoorthy^{ID}^{*b} and Shyam Biswas^{ID}^{*a}

In the present work, a new MOF material of the UiO-family called Zr-UiO-66-NH-CH₂-Py (**1**) has been obtained by the solvothermal technique and successfully characterized. The MOF structure was assembled with 2-((pyridin-4-ylmethyl) amino) terephthalic acid (H₂BDC-NH-CH₂-Py) as linker and Zr⁴⁺ ion. The activated form of **1** (called **1'**) exhibits considerable thermal and chemical stability. Compound **1'** showed a very rapid and selective response for the fluorometric sensing of superoxide (O₂^{•-}) in aqueous medium even in the presence of the potentially competitive reactive oxygen species (ROS). The limit of detection value for O₂^{•-} sensing is 0.21 μM, which is comparable with those of the reported O₂^{•-} sensors. This is the first MOF based fluorescent sensor for the detection of O₂^{•-}. The response time of this MOF sensor for O₂^{•-} is very short (240 s). On the other hand, **1'** was employed as a solid heterogeneous catalyst for Knoevenagel condensation between benzaldehyde and ethyl cyanoacetate at 80 °C in ethanol resulting in a very high yield of the desired product. The effects of the esterified linker ((CH₃)₂BDC-NH-CH₂-Py) and the corresponding metal salt (ZrCl₄) on this catalytic reaction were examined separately. We have also tested the substrate scope elaborately for the catalytic reaction promoted by catalyst **1'**.

Received 11th September 2019,
Accepted 18th October 2019

DOI: 10.1039/c9dt03638e

rsc.li/dalton

Introduction

Reactive oxygen species, which are generated endogenously mainly from the respiration of mitochondria^{1–3} and from oxygen species³ and exogenously upon exposure to UV light^{1,4} and infectious agents,^{1,4} are the origin of many biological processes such as inflammation,^{5,6} oxidative stress,⁵ oxidation of DNA and signal transduction,^{1,7} neurodegenerative injury,⁸ etc. Superoxide (O₂^{•-}) is a one-electron reduction species of molecular O₂, which damages biological membranes and tissues directly.^{9,10} The root of production of all ROS like H₂O₂, hypochlorite (OCl⁻), singlet oxygen (¹O₂), *t*-butyl hydroperoxide (TBHP), the hydroxyl radical (OH[•]) and the TBHP radical (TBHP[•]) is O₂^{•-}.^{11,12} Again, O₂^{•-} production is enhanced by

NADH via the NAD(P)H oxidase system.¹³ In biological systems, among all the ROS, O₂^{•-} is the primary ROS, which is responsible for cardiovascular disease and cancer and is also involved in cellular signal transduction.^{3,9,14–16} Some serious issues like oxidative chain reactions,¹⁷ hepatitis,¹⁸ degenerative disorders,³ and ischemia-reperfusion (IR) injury take place in surgery¹⁹ because of excess dosage of O₂^{•-} in living organisms. Hence, development of some analytical probes for the detection of endogenous and exogenous O₂^{•-} with excellent selectivity and sensitivity has great impacts on current research. In the last decades, many researchers have tried to prepare some probes including some organic probes,²⁰ hydroethidine (HE),²¹ and nanoscale coordination polymers (NCPs)²² for the fluorometric detection of O₂^{•-}. But, the disadvantages associated with these probes are poor stability, biotoxicity for cells, poor selectivity, and less efficiency due to their amorphous nature and smooth surface.^{23–25}

The Knoevenagel condensation reaction involves the formation of a substituted olefin using an aldehyde or a ketone and an active methylene compound in the presence of base as catalysts.^{26–30} This reaction is one of the familiar reactions for forming C–C bonds in organic transformations and often produces α,β-unsaturated ketones.^{26,29,31} Base catalyzed condensation reactions are some of the important reactions involved in the construction of molecules that can be used as

^aDepartment of Chemistry, Indian Institute of Technology Guwahati, 781039 Assam, India. E-mail: sbiswas@iitg.ac.in; Fax: +91-3612582349; Tel: +91-3612583309

^bSchool of Chemistry, Madurai Kamaraj University, Madurai 625021, Tamil Nadu, India. E-mail: admguru@gmail.com

† Electronic supplementary information (ESI) available: Materials and characterization methods, synthesis of the linker, mass, NMR and IR spectra, XRPD patterns, TG curves, N₂ sorption isotherms, fluorescence and UV-Vis spectra, GC-MS traces, the reusability plot for catalysis, and tables showing the unit cell parameters of **1**, detection limits and response times for O₂^{•-} sensing. See DOI: 10.1039/C9DT03638E

‡ These authors contributed equally to this work.

fine chemicals and drugs.^{26,32,33} Mostly, these reactions are performed using conventional homogeneous base catalysts such as amine, ammonia, pyridine, piperidine and alkali metal hydroxide which are poisonous and non-reusable and produce environmental waste.^{33,34} Henry reactions and Claisen–Schmidt reactions are also examples of organic condensation reactions which follow similar mechanistic protocols to Knoevenagel condensation using different types of nucleophiles.³⁵ But, use of these homogeneous catalysts for such types of condensation reactions leads to many problems such as undesired side reactions, necessity of higher temperature, poor loading of catalysts, reduced recyclability, consumption of longer time during work up and problems associated with catalyst recovery.^{32,33} In order to overcome these real problems, scientists have developed numerous heterogeneous catalysts like modified zeolites,³⁶ carbon nanotubes,³⁷ ionic liquids,³⁸ and Cu₃TATAT.³⁹ Still researchers are trying to develop some new heterogeneous catalysts which would be very easy to prepare and have high substrate scope, high stability and high recyclability.

Due to their distinctive qualities such as tunable pore sizes,⁴⁰ extraordinary surface areas,⁴¹ high thermal⁴² and chemical stability,⁴³ and tunable functionality,⁴⁴ metal-organic frameworks (MOFs) are being explored vastly for various applications like gas separation and storage,⁴⁵ heterogeneous catalysis,⁴⁶ drug delivery,⁴⁷ light harvesting materials,⁴⁸ etc. Luminescent MOF-based chemosensors have gained splendid research attention recently for detecting ions,^{49,50} explosives,^{51–53} pH,⁵⁴ gas molecules⁵⁵ and small molecules.⁵⁶ The prime advantages of luminescent MOFs (LMOFs) are their easy preparation, fast response and high sensitivity towards various toxic molecules using fluorescence techniques.

Herein, we present the solvothermal synthesis and complete characterization of a Zr(IV)-based UiO-66 MOF (**1**) containing a novel functional moiety attached to the linker. The activated compound **1'** was successfully employed for the aqueous phase detection of O₂^{•−} via turn-on fluorescence in the presence of competitive ROS. Compound **1'** exhibits similar selectivity and sensitivity (Limit of Detection (LOD) = 0.21 μM) to those found in the existing reports for the detection of O₂^{•−}. The response time of the present MOF for O₂^{•−} sensing is comparable or shorter than the reported probes.^{5,14,57–62} Probe **1'** is the first example for the MOF based detection of O₂^{•−}. Furthermore, **1'** was successfully employed for the Knoevenagel condensation between benzaldehyde and ethyl cyanoacetate at 80 °C with very high yield of the desired product. The functional moiety attached at the linker plays a significant role in the Knoevenagel condensation reaction, is quite new compared to the traditional functional groups used for the MOF based Knoevenagel condensation reaction.^{27,63–65} The substrate scope and the effects of the metal salt and the free linker on catalysis are described here. The reusability and heterogeneous characteristics of the material for the catalytic study make this catalyst very important and useful for practical applications.

Experimental section

Synthesis of [Zr₆O₄(OH)₄(BDC-C₆H₈N₂)₆]₂·5H₂O·1.5DMF (Zr-UiO-66-NH-CH₂-Py, **1**)

In a sealed glass tube, ZrCl₄ (35 mg, 0.15 mmol), the H₂BDC-NH-CH₂-Py linker (40 mg, 0.15 mmol), benzoic acid (538 mg, 4.5 mmol) and 2 mL of *N,N*-dimethylformamide (DMF) were taken and allowed to sonicate for 10 min. Afterwards, the sealed glass tube was heated at 120 °C for 24 h using a block heater and a yellow colored precipitate was obtained. The product was collected by vacuum filtration and acetone (3 × 2 mL) was used to wash the product. The solid material was dried at 70 °C for 4 h in a conventional oven. The yield was 49 mg (0.02 mmol, 81%) based on the Zr salt. Elem. anal. calcd for C_{88.5}H_{79.5}N_{13.5}O₃₆Zr₆ (2455.49 g mol^{−1}): C, 43.28; H, 3.26; N, 7.70%. Found: C, 43.65; H, 2.72; N, 7.28%. FT-IR (KBr, cm^{−1}): 3365 (br), 3065 (w), 2917 (w), 1688 (w), 1598 (s), 1567 (vs), 1504 (m), 1419 (s), 1383 (s), 1307 (m), 1288 (m), 1257 (vs), 1150 (m), 1068 (m), 1024 (m), 768 (vs), 719 (vs), 661 (vs), 571 (sh), 473 (s).

Activation of compound **1**

In a round bottom flask, 100 mg of compound **1** was stirred in 25 mL of methanol at room temperature. After 24 h, the solid material was collected by vacuum filtration and dried at 60 °C in a conventional oven for 4 h. In the next step, this compound was kept at 100 °C under high vacuum for 24 h. Thus, activated compound **1'** was achieved.

Preparation of the suspension of **1'** for fluorescence sensing experiments

As the fluorescence titration experiments need a stable suspension of the probe, 2 mg of **1'** was taken in a glass vial containing 3 mL of water, followed by sonication for 1 h. Then, it was kept under ambient conditions for 24 h to get a stable suspension for sensing experiments.

Fluorescence sensing experiments

For performing O₂^{•−} sensing experiments, 2900 μL of water and 100 μL of an aqueous suspension of **1'** were taken in a 3 mL quartz cuvette. Afterwards, a 10 mM aqueous solution of O₂^{•−} (KO₂ in water) was added in incremental volumes (30 μL at every addition) up to 180 μL. Fluorescence spectra were acquired after light excitation at 330 nm.

Reaction procedure for the catalytic study

To a reaction vessel containing a solution of aldehyde (0.5 mmol) and ethyl cyanoacetate (0.5 mmol) in ethanol (0.3 mL), the catalyst (20 mg, 1.7 mol%) was added. Then, this mixture was mixed homogeneously and placed in an oil bath maintaining the temperature at 80 °C for 12 h. The samples were aliquoted into a gas chromatograph (GC) to examine the progress of the reaction at different time intervals. Then, the conversion of the substrate to the product and its selectivity were checked by GC. Agilent GC was used to calculate the percentage yield of the product using the internal standard

method. The obtained products were characterized by the GC-MS technique. The same procedure was followed during the reusability experiments except that the catalyst was filtered from the reaction mixture, washed two times with dichloromethane and dried at 80 °C for 1 h. After drying, the catalyst was recycled for the reaction in the subsequent cycles with fresh aldehyde and ethyl cyanoacetate.

Results and discussion

Preparation and activation procedures

A yellow precipitate of **1** was obtained when a mixture of $ZrCl_4$, the $H_2BDC-NH-CH_2-Py$ (Fig. S1–S3, ESI†) linker, and benzoic acid (BA) was kept in a 1 : 1 : 30 molar ratio in a sealed glass tube and 3 mL of DMF was added to it, followed by heating the total mixture at 120 °C for 24 h.

To achieve the guest free form of **1**, we treated compound **1** with methanol for 24 h at room temperature. Afterwards, this methanol exchanged material was collected by vacuum filtration and heated at 100 °C under high vacuum for 24 h. Consequently, activated compound **1'** was achieved.

Infrared spectroscopy

The FT-IR spectra of the $H_2BDC-NH-CH_2-Py$ linker, as-synthesized (**1**) and activated (**1'**) compounds are shown in Fig. S4, ESI†. In the FT-IR spectrum of the free linker, the strong bands at 1580 and 1441 cm^{-1} are observed due to the asymmetric and symmetric stretching vibrations of the free carboxylic acid moiety. Two strong bands at 1567 and 1419 cm^{-1} are observed in the FT-IR spectra of **1** and **1'** due to the presence of the asymmetric and symmetric stretching frequencies of the coordinated carboxylate group of linker molecules, respectively. A band at 1688 cm^{-1} is observed in the FT-IR spectrum of the as-synthesized compound due to the presence of the carbonyl group of DMF molecules. This band is absent in the activated compound, which confirms that complete activation of **1** has been achieved successfully.

Thermal stability

Thermogravimetric (TG) analyses were performed from 25 to 700 °C under an argon atmosphere. As per the TG curve (Fig. S5, ESI†), the thermal stability of **1** is up to 340 °C.

The TG trace of **1** (Fig. S5, ESI†) displays three main steps of weight loss. From 25 to 130 °C, the first weight loss of 2.2 wt% occurs due to the elimination of 2.5 guest water molecules per formula unit (calcd: 1.8 wt%). From 130 to 340 °C, the second weight loss of 4.6 wt% occurs due to the removal of 1.5 occluded DMF molecules per formula unit (calcd: 4.4 wt%). The third weight loss was noticed at 340 °C due to the collapse of the framework and the decomposition of organic linkers. The weight loss of compound **1'** in the temperature range of 130–340 °C occurs due to the loss of water and DMF molecules (Fig. S5, ESI†). From 25 to 130 °C, the first weight loss of 1.2 wt% occurs due to the elimination of 1.5 guest water molecules per formula unit (calcd: 1.1 wt%).

From 130 to 340 °C, the second weight loss of 3.7 wt% occurs due to the removal of 1.2 occluded DMF molecules per formula unit (calcd: 3.6 wt%). The third weight loss was noticed at 345 °C due to the collapse of the framework and the elimination of organic linkers. Hence, it can be deduced that compound **1** was not completely activated. It can be mentioned that **1** and **1'** are well comparable with the reported Zr-based UiO-66 MOF materials in terms of thermal stability.^{66–71}

XRPD analysis

The XRPD patterns of **1** and **1'** are shown in Fig. 1. The XRPD patterns of **1** and **1'** are very similar to that of the simulated Zr-UiO-66 MOF (Fig. 1). We have also carried out the indexing of the XRPD pattern of as-synthesized **1** and the obtained unit cell parameters are given in Table S1 (ESI†). The results of this indexing are much close to those obtained for the reported UiO-66 MOF. Furthermore, a Pawley fit (Fig. S6, ESI†) of the XRPD pattern of **1** was performed, which exhibited excellent similarity with the simulated XRPD pattern of **1**. Therefore, it is very clear that as-synthesized **1** has the UiO-66 framework structure.^{72–74} Besides, it can be noticed that **1'** retains its structural robustness (as judged by its crystallinity) even after the activation process (Fig. 1). Therefore, **1** is stable under activation conditions.

Chemical stability

In order to check the chemical stability in water, 1 M HCl and glacial acetic acid, **1'** was stirred in these three liquids for 14 h. After that we collected the solid materials by vacuum filtration, dried them at 60 °C for 1 h and recorded their XRPD data. The XRPD data (Fig. S7, ESI†) reveal that the peak positions and intensities remained almost unaltered even after immersing **1'** in these three liquids, which confirmed that **1'** is stable enough in water, 1 M HCl and glacial acetic acid. The chemical

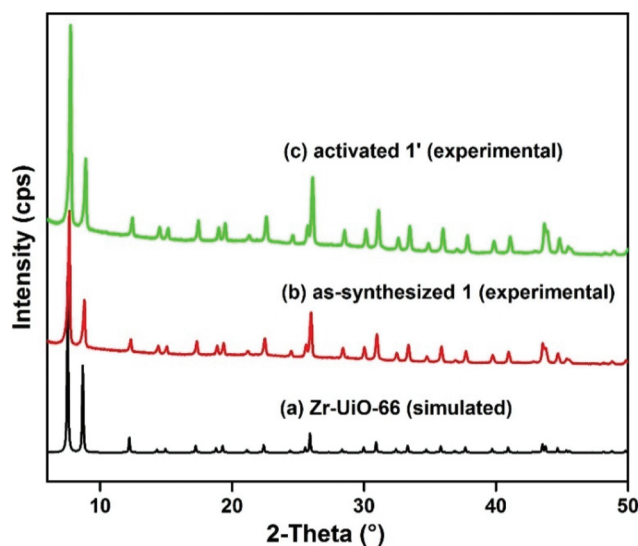


Fig. 1 XRPD patterns of (a) Zr-UiO-66 (simulated), (b) as-synthesized **1** (experimental) and (c) activated **1'** (experimental).

stability of compound **1'** was also checked in aqueous solutions of KOH at pH = 8, 10 and 12. After stirring in these three KOH solutions having different pH values for 16 h, the solid materials were collected by vacuum filtration and their XRPD data were recorded. The XRPD patterns (Fig. S8, ESI†) of these materials revealed that compound **1'** is moderately stable in aqueous solutions of KOH at pH = 8 and 10 but it completely lost its framework structure in the aqueous solution of KOH at pH = 12. The chemical stability of **1'** is well comparable with that of the previously reported UiO-66 MOFs.^{72,73,75}

N₂ sorption analysis

For investigating the nature and extent of porosity, we acquired the N₂ sorption isotherms of **1'** at -196 °C. The N₂ sorption curves (Fig. S9, ESI†) clearly indicate that **1'** is microporous (type I shape) in nature. The BET surface area was found to be 642 m² g⁻¹. The micropore volume at $p/p_0 = 0.5$ corresponded to 0.40 cm³ g⁻¹. The values of micropore volume and BET surface area are comparable with those of reported UiO-66 MOF materials.^{42,56,70,75}

Photoluminescence properties

The photoluminescence properties of both the free H₂BDC-NH-CH₂-Py linker and **1'** were studied in the solid state and aqueous medium. The results (Fig. S10 and S11, ESI†) indicate that the free H₂BDC-NH-CH₂-Py linker has much higher fluorescence intensity compared to that of **1'** in both the solid state and aqueous medium. In the solid-state luminescence study, the emission maxima for **1'** and the free H₂BDC-NH-CH₂-Py linker were found at 470 nm and 505 nm, respectively. In the case of aqueous medium, the emission maxima for **1'** and the free H₂BDC-NH-CH₂-Py linker were observed at 450 nm and 455 nm, respectively.

Sensing behavior towards O₂^{•-}

In order to investigate the potential ability of **1'** to sense O₂^{•-} in aqueous medium, we studied its fluorescence change upon treatment with O₂^{•-} solution. The suspension of **1'** (100 μL) was added to 2900 μL of water in a quartz cuvette. Afterwards, 10 mM aqueous solution of O₂^{•-} was added incrementally. The fluorescence intensity was saturated after the addition of 180 μL of O₂^{•-} solution. There was 100 fold increment in fluorescence intensity with a blue shift of emission maximum from 450 to 430 nm (Fig. 2 and 3).

For a smart sensor, selectivity for desired species is highly preferred. For this purpose, we tested the sensing ability of **1'** towards other ROS including HOCl, H₂O₂, OH[•], TBHP, TBHP[•], and ¹O₂. From Fig. 3 and Fig. S12–S17, ESI†, it is very clear that none of the ROS except O₂^{•-} caused considerable turn-on fluorescence upon addition to the suspension of **1'**. Therefore, **1'** exhibits high selectivity towards O₂^{•-}.

The sensing proficiency of **1'** towards O₂^{•-} with respect to time was studied by performing time dependent fluorescence sensing experiments. In order to perform these experiments, we poured 100 μL of the suspension of **1'** into a cuvette containing 2900 μL of water. Afterwards, 180 μL of a solution of

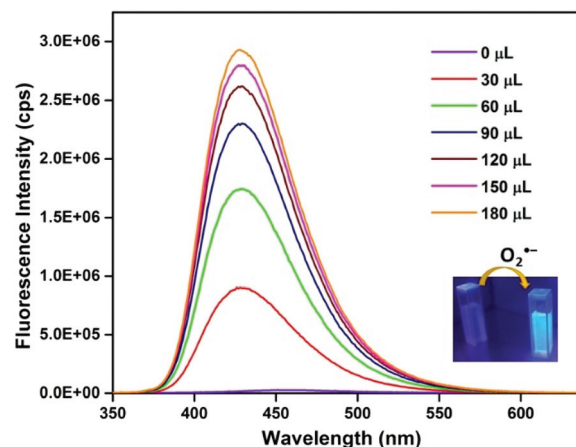


Fig. 2 Enhancement of the fluorescence response of **1'** upon stepwise addition of 10 mM aqueous solution of O₂^{•-} ($\lambda_{\text{ex}} = 330$ nm and $\lambda_{\text{em}} = 430$ nm). Inset: digital photographs of cuvettes containing aqueous suspension of **1'** before and after the addition of O₂^{•-} under UV-Vis lamp light.

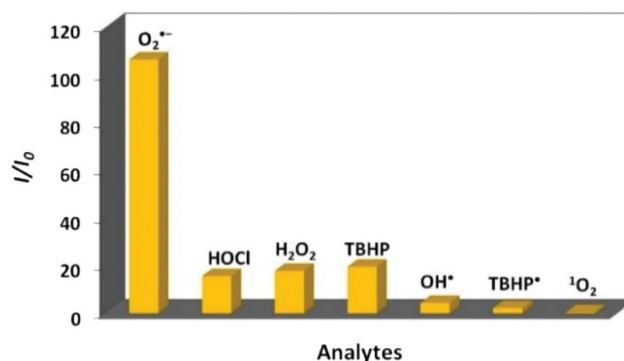


Fig. 3 Fluorescence enhancement of **1'** (aqueous suspension) upon treatment with 180 μL of 10 mM aqueous solution of various ROS.

O₂^{•-} was added. The fluorescence of **1'** was saturated within 240 s (Fig. 4).

The selectivity of **1'** towards O₂^{•-} in the presence of other potentially competitive ROS is highly required for practical applications. To check this ability, 180 μL of competing ROS solution (10 mM) was added to the suspension of **1'** and fluorescence spectra were acquired after 240 s. Thereafter, 180 μL of O₂^{•-} solution (10 mM) was added and fluorescence data were collected after 240 s. It was observed that there was negligible turn-on fluorescence response after the addition of competing ROS, whereas there was considerable fluorescence turn-on response after the addition of O₂^{•-}. All these results (Fig. 5 and Fig. S12–S17, ESI†) suggest that **1'** is highly selective towards O₂^{•-} only, even in the presence of other potentially competitive ROS.

The LOD for O₂^{•-} was calculated using the well-known formula: $\text{LOD} = 3\sigma/m$ (Fig. S18, ESI†).^{49,51,76} The LOD value was found to be 0.21 μM, which is comparable with those of other reported O₂^{•-} sensors (Table S2, ESI†).^{5,9,14,20,57,77}

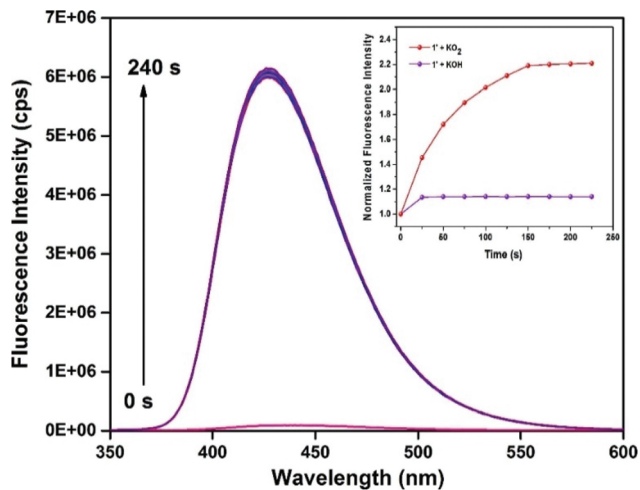


Fig. 4 Turn-on fluorescence response of **1'** with time upon treatment with 180 μL of 10 mM aqueous solution of $\text{O}_2^{\bullet-}$ ($\lambda_{\text{ex}} = 330 \text{ nm}$ and $\lambda_{\text{em}} = 430 \text{ nm}$). Inset: fluorescence kinetic spectra of **1'** upon treatment with 10 mM aqueous solutions of KO_2 (red) and KOH (violet).

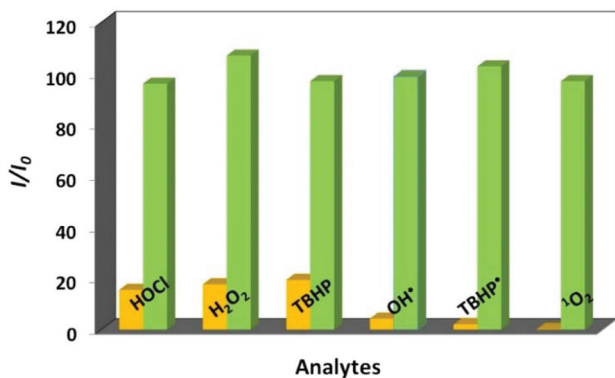


Fig. 5 Fluorescence enhancement of **1'** upon treatment with 180 μL of 10 mM aqueous solution of $\text{O}_2^{\bullet-}$ in the presence of other potentially competing ROS.

The recyclability experiments were conducted with **1'** up to three cycles. The compound was acquired by filtration and washed with water after every cycle of the sensing experiment. Compound **1'** showed no recyclability after the first cycle (Fig. S19, ESI[†]).

Mechanism for the sensing of $\text{O}_2^{\bullet-}$

To find out the mechanism for $\text{O}_2^{\bullet-}$ sensing in aqueous medium, XRPD, FT-IR, UV-Vis, and HR-MS analyses were carried out. From the recyclability study (Fig. S19, ESI[†]), it was observed that **1'** was not recyclable, which indicated that the reaction between **1'** and $\text{O}_2^{\bullet-}$ in aqueous medium led to the fluorescence turn-on properties. For XRPD and FT-IR analyses, samples of **1'** were treated with various concentrations of aqueous solutions of $\text{O}_2^{\bullet-}$. Afterwards, the solid materials were collected by filtration. The XRPD and FT-IR data of these solids were recorded. From the XRPD plots (Fig. S20 and S21,

ESI[†]), it was observed that the structure of **1'** was gradually destroyed upon treatment with increasing concentrations of $\text{O}_2^{\bullet-}$ in aqueous medium. FT-IR spectroscopy (Fig. S22, ESI[†]) also supported the structural collapse of **1'** in the presence of $\text{O}_2^{\bullet-}$ by showing a decrease in the peak intensity of stretching vibrations of **1'** with increasing concentration of $\text{O}_2^{\bullet-}$ in aqueous medium. Afterwards, UV-Vis spectra (Fig. S23, ESI[†]) were recorded for the free linker, the supernatant after treating **1'** with $\text{O}_2^{\bullet-}$ and the free linker after treatment with $\text{O}_2^{\bullet-}$. As the UV-Vis spectra of the supernatant after treatment of **1'** with $\text{O}_2^{\bullet-}$ and the $\text{O}_2^{\bullet-}$ -treated free linker are almost similar, we can conclude that the coordinated linker molecules were released from the framework of **1'** in aqueous medium upon treatment with $\text{O}_2^{\bullet-}$. The absorption maxima of the supernatant collected after treating **1'** with $\text{O}_2^{\bullet-}$ and the $\text{O}_2^{\bullet-}$ -treated free linker are blue shifted (Fig. S23, ESI[†]) due to the change in the pH value of the solvent system after the addition of KO_2 .^{78,79} In addition, we recorded the HR-MS spectrum of the filtrate after treatment of **1'** with $\text{O}_2^{\bullet-}$ solution. We observed a strong peak at $[m/z + \text{H}^+] = 273.0864$ (+ESI mode) (Fig. S24, ESI[†]), which corresponds to the linker molecule ($\text{H}_2\text{BDC-NH-CH}_2\text{-Py}$). Moreover, it is noticed from Fig. S11 (ESI[†]) that the $\text{H}_2\text{BDC-NH-CH}_2\text{-Py}$ linker has higher fluorescence intensity compared to that of **1'** in water. Hence, it can be inferred that the organic linker is released into the solution upon treatment of **1'** with $\text{O}_2^{\bullet-}$, which enhances the fluorescence intensity of the system. Consequently, a remarkable turn-on fluorescence signal was observed for **1'** in the presence of $\text{O}_2^{\bullet-}$.

Control experiments for $\text{O}_2^{\bullet-}$ sensing in the presence of KOH

As KO_2 can produce both $\text{O}_2^{\bullet-}$ and KOH in water, we performed control fluorescence experiments for $\text{O}_2^{\bullet-}$ sensing in the presence of 10 mM aqueous KOH solution. In one set of experiments, 180 μL of 10 mM $\text{O}_2^{\bullet-}$ solution was added to the aqueous suspension of **1'** followed by the addition of 180 μL of 10 mM KOH solution (Fig. S25, ESI[†]). In another set of experiments, 180 μL of 10 mM KOH solution was added to the aqueous suspension of **1'** followed by the addition of 180 μL of 10 mM $\text{O}_2^{\bullet-}$ solution (Fig. S26, ESI[†]). In both cases, turn-on fluorescence responses were observed. However, XRPD analysis showed that the framework structure of **1'** was lost partially after treatment with 10 mM aqueous KOH solution (Fig. S27, ESI[†]), whereas the framework of **1'** was lost completely after treatment with 10 mM aqueous $\text{O}_2^{\bullet-}$ solution under sensing conditions (Fig. S21, ESI[†]). Moreover, the fluorescence kinetics plots of **1'** (Fig. S28, ESI[†]) after treatment with 10 mM aqueous KOH and $\text{O}_2^{\bullet-}$ solutions showed that the saturation time is much faster in the presence of KOH (30 s) than in the presence of $\text{O}_2^{\bullet-}$ (240 s). Hence, from the above results, it can be concluded that fluorescence turn-on was observed due to the presence of $\text{O}_2^{\bullet-}$ and KOH produced in the sensing medium during the generation of $\text{O}_2^{\bullet-}$.

Catalytic activity in Knoevenagel condensation

Knoevenagel condensation produces unsaturated compounds upon nucleophilic addition of a carbanion to an electrophilic

carbonyl group by removal of a water molecule. This is one of the most classical organic reactions and has received wide interest due to the importance of condensation products as therapeutic drugs, natural products, heterocyclic compounds, and fine chemicals. The Knoevenagel condensation reaction was reported conventionally using a series of base catalysts like piperidine, morpholine, triethylamine, KF and K_2CO_3 . Furthermore, this condensation reaction has been reported using a series of heterogeneous solid base catalysts with obvious advantages of recovery and reusability. In recent years, the Knoevenagel condensation reaction between active methylene and carbonyl compounds has also been investigated using MOFs as heterogeneous solid catalysts such as $Zn_2(tpt)_2(2-atp)I_2$,⁸⁰ MOF-NH₂,⁸¹ Al-MIL-101-NH₂,⁸² IRMOF-3,⁸³ $Cu_3(BTC)_2/Fe(BTC)$,⁸⁴ and Hf-UiO-66-N₂H₃.⁷⁸

The catalytic activity of **1'** was investigated by selecting benzaldehyde and ethyl cyanoacetate as model substrates and the reaction conditions were optimized in terms of solvent, reaction temperature and catalyst loading. The obtained products were characterized by the GC-MS technique (Fig. S29–S44, ESI†). A blank control experiment between benzaldehyde and ethyl cyanoacetate without a catalyst resulted in 23% yield at 80 °C in ethanol after 12 h. Furthermore, the reaction of benzaldehyde and ethyl cyanoacetate was performed using **1'** with different loadings. The observed results are presented in Fig. 6. This figure clearly indicates that the reaction was significantly promoted to provide an optimum yield of 94% with 1.7 mol% catalyst loading compared to other catalyst loadings. Hence, further reactions were performed with this catalyst loading. Similarly, the reaction of benzaldehyde and ethyl cyanoacetate in the presence of **1'** was screened with various organic solvents like acetonitrile, dichloroethane, toluene and xylene. The experimental results are displayed in Table 1. The catalytic data using **1'** as the catalyst in the above-mentioned solvents indicate that ethanol is the preferred solvent to achieve higher yield of the Knoevenagel condensation product.

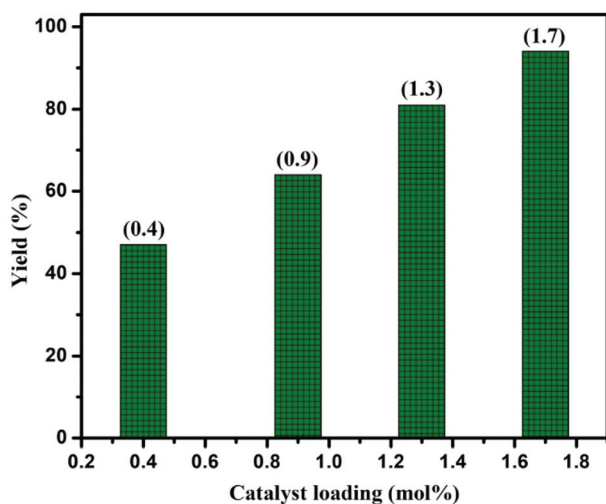


Fig. 6 The effect of catalyst loading on the Knoevenagel condensation reaction between benzaldehyde and ethyl cyanoacetate in ethanol.

Table 1 Optimization of reaction conditions for the Knoevenagel condensation reaction between benzaldehyde and ethyl cyanoacetate using MOF **1'** as the heterogeneous solid catalyst^a

Entry	Catalyst	T (°C)	Solvent	Yield (%) ^b
1 ^c	—	80	Ethanol	23
2	1'	80	Ethanol	94(81)
3	1'	80	Acetonitrile	39
4	1'	80	Dichloroethane	18
5	1'	80	Toluene	31
6	1'	80	Xylene	38
7 ^d	1'	80	Ethanol	54
8 ^e	1'	80	Ethanol	35
9	1'	60	Ethanol	56
10	1'	40	Ethanol	27
11 ^f	1'	80	Ethanol	64
12 ^g	H ₂ BDC-NH-CH ₂ -Py linker	80	Ethanol	85
13 ^h	(CH ₃) ₂ BDC-NH-CH ₂ -Py linker	80	Ethanol	88
14 ⁱ	ZrCl ₄	80	Ethanol	33
15	Zr-UiO-66	80	Ethanol	63
16	Zr-UiO-66-NH ₂	80	Ethanol	89

^a Reaction conditions: benzaldehyde (0.5 mmol), ethyl cyanoacetate (0.5 mmol), catalyst (20 mg, 1.7 mol%), solvent (0.3 mL), 80 °C, 12 h. ^b Yields were determined by GC. The value in parentheses indicates the catalytic activity of **1'**. ^c The blank experiment in the absence of a catalyst. ^d Performed with 1 mL of solvent under stirring. ^e Performed with 2 mL of solvent under stirring. ^f Catalyst loading was 10 mg (0.9 mol%). ^g 13.5 mg (9.9 mol%) of the linker was used. ^h 13.5 mg (8.9 mol%) of the ester linker was used. ⁱ 11.5 mg (9.8 mol%) of the metal salt was used.

Furthermore, the reaction between benzaldehyde and ethyl cyanoacetate using MOF **1'** as the catalyst showed lower yield when ethanol was used in excess amounts compared to the optimized reaction conditions. In addition, the reaction between benzaldehyde and ethyl cyanoacetate was performed in the presence of **1'** at 60 and 40 °C in ethanol and the respective yields of the desired products were 56 and 27%. Fig. 7 portrays the effect of reaction temperature on the reaction between benzaldehyde and ethyl cyanoacetate using **1'** as the solid catalyst. These catalytic data suggest that higher yield of the product is found only at higher reaction temperature. Furthermore, the activity of **1'** was compared with those of the respective metal salts and the organic linker. The experimental results are shown in Table 1. The reaction of benzaldehyde with ethyl cyanoacetate in the presence of the (CH₃)₂BDC-NH-CH₂-Py linker as a homogeneous catalyst resulted in a yield which is comparable to **1'**, whereas the H₂BDC-NH-CH₂-Py linker showed 85% yield at 80 °C in ethanol. These catalytic data clearly indicate that the pyridine moiety in the linker acts as a catalytic site and the superior activity of the (CH₃)₂BDC-NH-CH₂-Py linker is due to the absence of self-quenching of basic sites in the free linker. In contrast, this reaction exhibited only 33% yield using ZrCl₄ as a homogeneous control catalyst under identical reaction conditions. On the other hand, the catalytic performance of **1'**

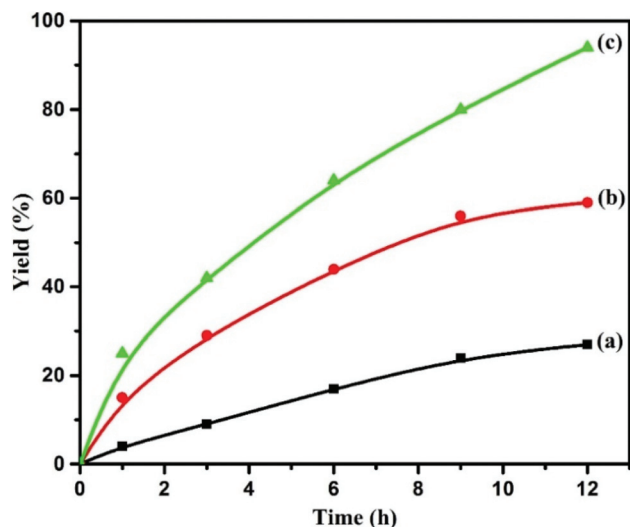


Fig. 7 The effect of temperature on the Knoevenagel condensation reaction between benzaldehyde and ethyl cyanoacetate using **1'** as the solid catalyst at (a) 40 °C, (b) 60 °C and (c) 80 °C.

(without any activation) and **1'** was compared for the above reaction under similar conditions to reveal the effect of activation. The results indicate that the prior activation of **1** has a strong influence on the catalytic activity as shown in Fig. 8 and Table 1. Comparison of the activity of **1'** with its related metal salt and the methyl ester of the organic linker shows that MOF **1'** exhibits better activity than the methyl ester of the organic linker and the metal salt (Fig. 8). Furthermore, it is clearly proved that the active site promoting this reaction under optimized reaction conditions is the basic functionality available in the organic linker compared to the metal center. This hypothesis was further confirmed by comparing the activity of

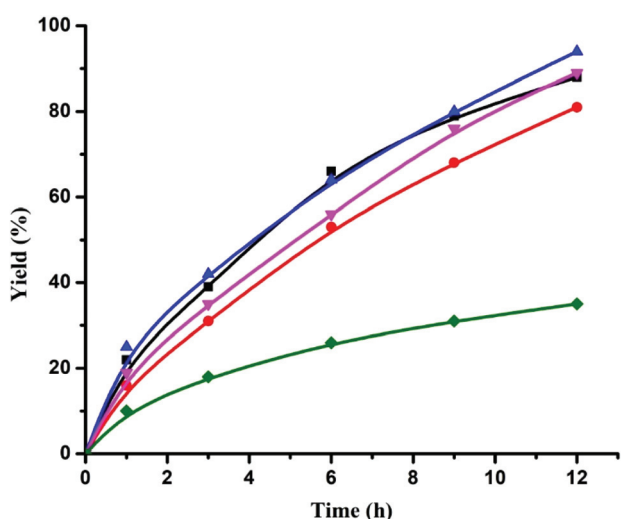


Fig. 8 Time yield plots for the Knoevenagel condensation reaction between benzaldehyde and ethyl cyanoacetate using **1'** (▲), the (CH₃)₂BDC-NH-CH₂-Py linker (■), Zr-UiO-66-NH₂ (▼), **1** (●), and ZrCl₄ (◆).

1' with the Zr-UiO-66-NH₂ MOF under identical conditions (Fig. 8). These catalytic data clearly indicate that **1'** exhibits a slightly better activity than Zr-UiO-66-NH₂. In contrast, Zr-UiO-66 without any basic sites showed much lower activity than **1'** and Zr-UiO-66-NH₂ solids under similar conditions. Hence, these results prove that the basic functionality in the linker is essential to achieve higher yield of the condensation product.

Fig. 9 shows the time conversion plot for the Knoevenagel condensation between benzaldehyde and ethyl cyanoacetate in the presence of **1'** as the catalyst with minimal amounts of ethanol as shown in Table 1. One of the important control experiments in heterogeneous catalysis is to check the heterogeneity of the reaction. This control study was performed by the leaching or hot-filtration experiment. As shown in Fig. 9, the reaction was started under optimized reaction conditions. Later, the catalyst was filtered at reaction temperature after 1 h and the reaction of the resulting reaction mixture in the absence of the solid catalyst was continued further for 11 h. Samples were periodically collected and analyzed by GC. The comparison of the kinetic profiles with and without the solid catalyst indicates that the reaction is heterogeneous in nature.

Recovery and reuse of the catalyst in consecutive reaction cycles are the key aspects of developing new heterogeneous catalysts. In this aspect, the reusability of **1'** was investigated in the reaction between benzaldehyde and ethyl cyanoacetate under optimized reaction conditions. Fig. S45 (ESI[†]) displays the reusability results of **1'** as a solid base catalyst in promoting Knoevenagel condensation up to five cycles. It can be seen from this figure that the activity of the catalyst slightly decreased from the first cycle to the fifth cycle and this may be due to the catalyst loss (during filtration) in every cycle. Furthermore, the XRPD pattern of fresh **1'** was compared with

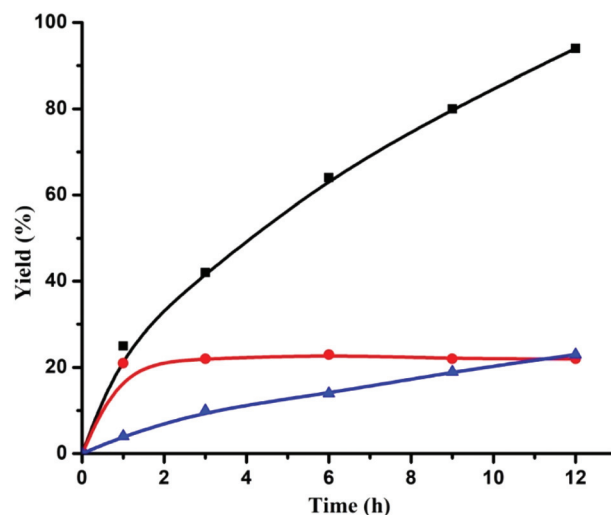


Fig. 9 The time conversion profile for the Knoevenagel condensation reaction between benzaldehyde and ethyl cyanoacetate: (■) in the presence of the catalyst, (●) hot filtration experiment upon filtration of the catalyst after 1 h from the reaction mixture excluding the contribution from blank control and (▲) the catalyst-free control experiment.

Table 2 Knoevenagel condensation reaction between various aldehydes and ethyl cyanoacetate in the presence of **1'** as a heterogeneous solid base catalyst^a

Entry	Aldehyde	Product	Yield (%) ^b
1			94
2			93
3			88
4			92
5			89
6			88
7			93
8			74
9			58
10			65
11			92
12			73
13			48
14			74

Table 2 (Contd.)

Entry	Aldehyde	Product	Yield (%) ^b
15			70
16			44

^a Reaction conditions: aldehyde (0.5 mmol), ethyl cyanoacetate (0.5 mmol), **1'** (20 mg, 1.7 mol%), ethanol (0.3 mL), 80 °C, 12 h.
^b Yields were determined by GC.

that of **1'** used in five cycles (Fig. S46, ESI[†]). These XRPD patterns indicate that the crystallinity of **1'** is not altered throughout the course of the reaction and the catalyst is highly robust under the present reaction conditions. In addition, the hot filtration experiment also proved the stability of the catalyst. Moreover, the FE-SEM images of **1** and **1'** before and after catalysis (Fig. S47–S49, ESI[†]) showed that the morphology of the nanocrystals of **1** remained unaffected after thermal activation and catalytic cycles during the recyclability experiments. Hence, all these available catalytic data, XRPD patterns and FE-SEM images suggest the stability of **1'** during the Knoevenagel condensation reaction under the present experimental conditions.

These preliminary catalytic data prompted us to examine the substrate scope of **1'** as a solid base catalyst with a wide range of substituted benzaldehydes containing electron withdrawing and electron donating groups. The obtained catalytic data are presented in Table 2. The reaction of 4-methylbenzaldehyde and 4-methoxybenzaldehyde with ethyl cyanoacetate using **1'** as the catalyst provided 93 and 88% yields of condensation products, respectively. On the other hand, 4-fluoro, 4-chloro, 4-bromo and 4-nitrobenzaldehydes reacted conveniently with ethyl cyanoacetate in the presence of **1'** to afford 92, 89, 88 and 93% yields, respectively. The reaction of 4-*tert*-butylbenzaldehyde with ethyl cyanoacetate in the presence of **1'** resulted in 74% yield under identical reaction conditions. Similarly, di- and tri-substituted benzaldehydes reacted with ethyl cyanoacetate, but the yields of the products reduced significantly under identical conditions. These catalytic data infer that these bulky benzaldehydes may experience diffusion limitations in reaching the active sites in **1'**. Furthermore, heterocyclic aldehydes like 2-furfural condensed with ethyl cyanoacetate in the presence of **1'** to afford 92% yield. On the other hand, salicylaldehyde and phenylacetaldehyde reacted with ethyl cyanoacetate to give the desired products in 73 and 48% yields, respectively. An α,β -unsaturated substrate like cinnamaldehyde also reacted with ethyl cyanoacetate in the presence of **1'** to provide 74% yield. Finally,

1-naphthaldehyde and 9-anthracenecarboxaldehyde were subjected to Knoevenagel condensation with ethyl cyanoacetate in the presence of **1'** leading to 70 and 44% yields of the respective condensed products. From these data, it is undoubtedly clear that the reaction is highly influenced by the molecular dimensions of aldehydes. These results clearly show that the condensation reaction occurs within the pores of **1'** and this is an interesting example to demonstrate the size-selective catalysis of MOF **1'** convincingly.

Conclusions

In this work, a new Zr-UiO-66 MOF (**1**) with the 2-((pyridin-4-ylmethyl) amino) terephthalic acid linker has been prepared with high crystallinity and thoroughly characterized. The MOF showed excellent thermal and chemical stability. The guest-free material (**1'**) displayed a considerable BET surface area (642 m² g⁻¹). Material **1'** was successfully employed for the turn-on fluorometric detection of O₂^{•-} in aqueous medium with high selectivity. The LOD (0.21 μM) of **1'** is comparable with those of the reported O₂^{•-} sensors. Remarkably, the response time (240 s) for O₂^{•-} is very fast. In addition, solid **1'** was effectively utilized as a solid heterogeneous catalyst for Knoevenagel condensation between benzaldehyde and ethyl cyanoacetate. The solid catalyst was used for five cycles with no appreciable decay in its performance and the hot filtration experiment indicated the heterogeneity of the process. Catalyst **1'** showed wide substrate scope in the construction of the C–C bond with high yields of Knoevenagel condensation products at 80 °C in ethanol. The catalyst also showed size selectivity indicating that the reaction occurs within the pores of the solid catalyst.

Conflicts of interest

There are no conflicts to declare.

Acknowledgements

AD and SB are grateful for financial assistance from the Science and Engineering Research Board, New Delhi via grant no. EMR/2016/006500 and EEQ/2016/000012, respectively. AD thanks the University Grants Commission, New Delhi, for the award of an Assistant Professorship under its Faculty Recharge Programme.

Notes and references

- M. Hayyan, M. A. Hashim and I. M. AlNashef, *Chem. Rev.*, 2016, **116**, 3029–3085.
- P. Li, W. Zhang, K. Li, X. Liu, H. Xiao, W. Zhang and B. Tang, *Anal. Chem.*, 2013, **85**, 9877–9881.
- M. Hayyan, M. A. Hashim and I. M. A. Nashef, *Chem. Rev.*, 2016, **116**, 3029–3085.
- N. Caporaso, *J. Natl. Cancer Inst.*, 2003, **95**, 1263–1265.
- J. Yang, X. Liu, H. Wang, H. Tan, X. Xie, X. Zhang, C. Liu, X. Qu and J. Hua, *Analyst*, 2018, **143**, 1242–1249.
- M. Majzunova, I. Dovinova, M. Barancik and J. Y. H. Chan, *J. Biomed. Sci.*, 2013, **20**, 69–79.
- C. M. Bergamini, S. Gambetti, A. Dondi and C. Cervellati, *Curr. Pharm. Des.*, 2004, **10**, 1611–1626.
- B. M. Babior, *Am. J. Med.*, 2000, **109**, 33–44.
- Y. Song, J. Hao, D. Hu, M. Zeng, P. Li, H. Li, L. Chen, H. Tan and L. Wang, *Sens. Actuators, B*, 2017, **238**, 938–944.
- W. M. Nauseef, *J. Immunol.*, 2014, **193**, 5357–5358.
- B. C. Dickinson and C. J. Chang, *Nat. Chem. Biol.*, 2011, **7**, 504–511.
- I. A. Abreu and D. E. Cabelli, *Biochim. Biophys. Acta, Proteins Proteomics*, 2010, **1804**, 263–274.
- R. A. Beswick, A. M. Dorrance, R. Leite and R. C. Webb, *Hypertension*, 2011, **38**, 1107–1111.
- Y. Xuan and J. Qu, *RSC Adv.*, 2018, **8**, 4125–4129.
- S. Dikalov, K. K. Griendling and D. G. Harrison, *Hypertension*, 2007, **49**, 717–727.
- P. Huang, L. Feng, E. A. Oldham, M. J. Keating and W. Plunkett, *Nature*, 2000, **407**, 390–395.
- Y. Sheng, I. A. Abreu, D. N. Cabelli, M. J. Maroney, A. F. Miller, M. Teixeira and J. S. Valentine, *Chem. Rev.*, 2014, **114**, 3854–3918.
- L. Wang, W. Wen, H. Xiong, X. Zhang, H. Gu and S. Wang, *Anal. Chim. Acta*, 2013, **758**, 66–71.
- L. L. Qu, D. W. Li, L. X. Qin, J. Mu, J. S. Fossey and Y. T. Long, *Anal. Chem.*, 2013, **85**, 9549–9555.
- D. Lu, L. Zhou, R. Wang, X.-B. Zhang, L. He, J. Zhang, X. Hu and W. Tan, *Sens. Actuators, B*, 2017, **250**, 259–266.
- H. Zhao, S. Kalivendi, H. Zhang, J. Joseph, K. Nithipatikom, J. Vásquez-Vivar and B. Kalyanaraman, *Free Radical Biol. Med.*, 2003, **34**, 1359–1368.
- N. Liu, J. Hao, K. Cai, M. Zeng, Z. Huang, L. Chen, B. Peng, P. Li, L. Wang and Y. Song, *Luminescence*, 2017, **33**, 119–124.
- S. Yang, X. Zhu, S. Zhou, S. Wang, Z. Feng, Y. Wei, H. Miao, L. Guo, F. Wang, G. Zhang, X. Gua and X. Mu, *Dalton Trans.*, 2014, **43**, 2521–2533.
- R. C. Huxford, K. E. Dekrafft, W. S. Boyle, D. Liu and W. Lin, *Chem. Sci.*, 2012, **3**, 198–204.
- J. Zielonka and B. Kalyanaraman, *Free Radicals Biol. Med.*, 2010, **48**, 983–1001.
- A. Dhakshinamoorthy, N. Heidenreich, D. Lenzen and N. Stock, *CrystEngComm*, 2017, **19**, 4187–4193.
- Y. Yang, H.-F. Yao, F.-G. Xi and E.-Q. Gao, *J. Mol. Catal. A: Chem.*, 2014, **390**, 198–205.
- M. J. Climent, A. Corma, I. Domínguez, S. Iborra, M. J. Sabater and G. Sastre, *J. Catal.*, 2007, **246**, 136–146.
- Y. Luan, Y. Qi, H. Gao, R. S. Andriamitantsoa, N. Zheng and G. Wang, *J. Mater. Chem. A*, 2015, **3**, 17320–17331.
- B. Parmar, P. Patel, V. Murali, Y. Rachuri, R. I. Kureshy, N.-U. H. Khan and E. Suresh, *Inorg. Chem. Front.*, 2018, **5**, 2630–2640.

- 31 L. F. Tietze, *Chem. Rev.*, 1996, **96**, 115–136.
- 32 E. M. Schneider, M. Zeltner, N. Kränzlin, R. N. Grass and W. J. Stark, *Chem. Commun.*, 2015, **51**, 10695–10698.
- 33 X. Zhang, E. S. M. Lai, R. M. Aranda and K. L. Yeung, *Appl. Catal., A*, 2004, **261**, 109–118.
- 34 R. Xing, H. Wu, X. Li, Z. Zhao, Y. Liu, L. Chen and P. Wu, *J. Mater. Chem.*, 2009, **19**, 4004–4011.
- 35 J. M. Concellón, P. L. Bernad, H. Rodriguez-Solla and C. Concellón, *J. Org. Chem.*, 2007, **72**, 5421–5423.
- 36 N. Elazarifi, A. Ezzamarty, J. Leglise, L. C. Menorval and C. Moreau, *Appl. Catal., A*, 2004, **267**, 235–240.
- 37 A. Villa, J. P. Tessonier, O. Majoulet, D. S. Su and R. Schlögl, *ChemSusChem*, 2010, **3**, 241–245.
- 38 B. C. Ranu and R. Jana, *Eur. J. Org. Chem.*, 2006, 3767–3770.
- 39 Z. Miao, Y. Luan, C. Qi and D. Ramella, *Dalton Trans.*, 2016, **45**, 13917–13924.
- 40 J. Zheng, R. S. Vemuri, L. Estevez, P. K. Koech, T. Varga, D. M. Camaioni, T. A. Blake, B. P. McGrail and R. K. Motkuri, *J. Am. Chem. Soc.*, 2017, **139**, 10601–10604.
- 41 R. Grünker, V. Bon, P. Müller, U. Stoeck, S. Krause, U. Mueller, I. Senkovska and S. Kaskel, *Chem. Commun.*, 2014, **50**, 3450–3452.
- 42 J. H. Cavka, S. Jakobsen, U. Olsbye, N. Guillou, C. Lamberti, S. Bordiga and K. P. Lillerud, *J. Am. Chem. Soc.*, 2008, **130**, 13850–13851.
- 43 J. Wang, Y. Li, M. Jiang, Y. Liu, L. Zhang and P. Wu, *Chem. – Eur. J.*, 2016, **22**, 13023–13027.
- 44 D. F. S. Gallis, L. E. S. Rohwer, M. A. Rodriguez, M. C. Barnhart-Dailey, K. S. Butler, T. S. Luk, J. A. Timlin and K. W. Chapman, *ACS Appl. Mater. Interfaces*, 2017, **9**, 22268–22277.
- 45 B. Li, H.-M. Wen, W. Zhou and B. Chen, *J. Phys. Chem. Lett.*, 2014, **5**, 3468–3479.
- 46 M. Karimi, T. Hajiashrafi, A. Heydari and A. A. Tehrani, *Appl. Organomet. Chem.*, 2017, **31**, e3866.
- 47 L. Wang, M. Zheng and Z. Xie, *J. Mater. Chem. B*, 2018, **6**, 707–717.
- 48 M. C. So, G. P. Wiederrecht, J. E. Mondloch, J. T. Hupp and O. K. Farha, *Chem. Commun.*, 2015, **51**, 3501–3510.
- 49 A. Das, S. Banesh, V. Trivedi and S. Biswas, *Dalton Trans.*, 2018, **47**, 2690–2700.
- 50 Y. Rachuri, B. Parmar, K. K. Bisht and E. Suresh, *Cryst. Growth Des.*, 2017, **17**, 1363–1372.
- 51 A. Das and S. Biswas, *Sens. Actuators, B*, 2017, **250**, 121–131.
- 52 B. Parmar, Y. Rachuri, K. K. Bisht, R. Laiya and E. Suresh, *Inorg. Chem.*, 2017, **56**, 2627–2638.
- 53 Y. Rachuri, B. Parmar, K. K. Bisht and E. Suresh, *Dalton Trans.*, 2016, **45**, 7881–7892.
- 54 Q. Meng, X. Xin, L. Zhang, F. Dai, R. Wang and D. Sun, *J. Mater. Chem. A*, 2015, **3**, 24016–24021.
- 55 M. Wang, L. Guo and D. Cao, *Anal. Chem.*, 2018, **90**, 3608–3614.
- 56 M. SK, S. Nandi, R. K. Singh, V. Trivedi and S. Biswas, *Inorg. Chem.*, 2018, **57**, 10128–10136.
- 57 K. Xu, X. Liu and B. Tang, *ChemBioChem*, 2007, **8**, 453–458.
- 58 F. Si, Y. Liu, K. Yan and W. Zhong, *Chem. Commun.*, 2015, **51**, 7931–7934.
- 59 H. Maeda, K. Yamamoto, Y. Nomura, I. Kohno, L. Hafsi, N. Ueda, S. Yoshida, M. Fukuda, Y. Fukuyasu, Y. Yamauchi and N. Itoh, *J. Am. Chem. Soc.*, 2005, **127**, 68–69.
- 60 R.-Q. Li, Z.-Q. Mao, L. Rong, N. Wu, Q. Lei, J.-Y. Zhu, L. Zhuang, X.-Z. Zhang and Z.-H. Liu, *Biosens. Bioelectron.*, 2017, **87**, 73–80.
- 61 D. P. Murale, H. Kim, W. S. Choi and D. G. Churchill, *Org. Lett.*, 2013, **15**, 3946–3949.
- 62 Y. Zhou, J. Ding, T. Liang, E. S. Abdel-Halim, L. Jiang and J.-J. Zhu, *ACS Appl. Mater. Interfaces*, 2016, **8**, 6423–6430.
- 63 Y. Yang, H.-F. Yao, F.-G. Xi and E.-Q. Gao, *J. Mol. Catal. A: Chem.*, 2014, **390**, 198–205.
- 64 A. R. Burgoyne and R. Meijboom, *Catal. Lett.*, 2013, **143**, 563–571.
- 65 B. Bhattacharya, D. K. Maity, P. Pachfule, E. Colacio and D. Ghoshal, *Inorg. Chem. Front.*, 2014, **1**, 414–425.
- 66 M. SK, M. R. U. Z. Khan, A. Das, S. Nandi, V. Trivedi and S. Biswas, *Dalton Trans.*, 2019, **48**, 12615–12621.
- 67 A. Das, S. Das, V. Trivedi and S. Biswas, *Dalton Trans.*, 2019, **48**, 1332–1343.
- 68 D. Bůzek, J. Demel and K. Lang, *Inorg. Chem.*, 2018, **57**, 14290–14297.
- 69 D. Cunha, C. Gaudin, I. Colinet, P. Horcajada, G. Maurin and C. Serre, *J. Mater. Chem. B*, 2013, **1**, 1101–1108.
- 70 S. Nandi, S. Banesh, V. Trivedi and S. Biswas, *Analyst*, 2018, **143**, 1482–1491.
- 71 S. Biswas and P. V. D. Voort, *Eur. J. Inorg. Chem.*, 2013, **2013**, 2154–2160.
- 72 M. Kandiah, M. H. Nilsen, S. Usseglio, S. Jakobsen, U. Olsbye, M. Tilset, C. Larabi, E. A. Quadrelli, F. Bonino and K. P. Lillerud, *Chem. Mater.*, 2010, **22**, 6632–6640.
- 73 Y. Huang, W. Qin, Z. Li and Y. Li, *Dalton Trans.*, 2012, **41**, 9283–9285.
- 74 F. Yang, W. Li and B. Tang, *J. Alloys Compd.*, 2018, **733**, 8–14.
- 75 S. Biswas and P. V. D. Voort, *Eur. J. Inorg. Chem.*, 2013, **2013**, 2154–2160.
- 76 S. Nandi and S. Biswas, *Dalton Trans.*, 2019, **48**, 9266–9275.
- 77 J. J. Gao, K. H. Xu, B. Tang, L. L. Yin, G. W. Yang and L. G. An, *FEBS J.*, 2007, **274**, 1725–1733.
- 78 A. Das, N. Anbu, A. Dhakshinamoorthy and S. Biswas, *Microporous Mesoporous Mater.*, 2019, **284**, 459–467.
- 79 P. Cheruku, J.-H. Huang, H.-J. Yen, R. S. Iyer, K. D. Rector, J. S. Martinez and H.-L. Wang, *Chem. Sci.*, 2015, **6**, 1150–1158.
- 80 Y. Tan, Z. Fu and J. Zhang, *Inorg. Chem. Commun.*, 2011, **14**, 1966–1970.
- 81 A. Taher, D.-J. Lee, B.-K. Lee and I.-M. Lee, *Synlett*, 2016, **27**, 1433–1437.
- 82 M. Hartmann and M. Fischer, *Microporous Mesoporous Mater.*, 2012, **164**, 38–43.
- 83 J. Gascon, U. Aktay, M. D. Hernandez-Alonso, G. P. M. V. Klink and F. Kapteijn, *J. Catal.*, 2009, **261**, 75–87.
- 84 M. Opanasenko, A. Dhakshinamoorthy, M. Shamzhy, P. Nachtigall, M. Horáček, H. Garcia and J. Čejka, *Catal. Sci. Technol.*, 2013, **3**, 500–507.